sciendo

TATRA MOUNTAINS
Mathematical Publications
DOI: 10.2478/tmmp-2020-0005
Tatra Mt. Math. Publ. **75** (2020), 63–80

THE FINITE ELEMENT METHOD AS A TOOL TO SOLVE THE OBLIQUE DERIVATIVE BOUNDARY VALUE PROBLEM IN GEODESY

Marek Macák — Zuzana Minarechová — Róbert Čunderlík — Karol Mikula

Slovak University of Technology in Bratislava, Bratislava, SLOVAKIA

ABSTRACT. In this paper, we propose a novel approach to approximate the solution of the Laplace equation with an oblique derivative boundary condition by the finite element method. We present and analyse diverse testing experiments to study its behaviour and convergence. Finally, the usefulness of this approach is demonstrated by using it to gravity field modelling, namely, to approximate the solution of a geodetic boundary value problem in Himalayas.

1. Introduction

A detailed knowledge and analysis of the Earth's gravity field is one of the main tasks of geodesy and it has been of interest of many researchers and working groups. As a result, there have been invented and developed various approaches to its determination. In this section, some key concepts are concisely given.

A determination of the Earth's gravity field is formulated in terms of the geodetic boundary value problems (BVPs). A combination of terrestrial gravimetric measurements and precise 3D positioning by GNSS (Global Navigation Satellite System) directly yields gravity disturbances, i.e., the oblique derivative boundary conditions (BC) of the fixed gravimetric boundary value problem (FGBVP). Therefore, from the mathematical point of view, the FGBVP represents an exterior oblique derivative geodetic BVP for the Laplace equation, cf. Koch and Pope [24], Freeden and Kersten [14], Bjerhammar and Svensson [5], Holota [20].

2010 Mathematics Subject Classification: 65N30.
Keywords: oblique derivative boundary value problem, finite element method.
Our research was supported by the grants APVV-15-0522 and VEGA 1/0486/20.

A standard procedure to solve the oblique derivative BVP has been based on integral equations using the single-layer potential, cf. Bitzadse [4], Miranda [36]. Koch and Pope [24] applied such an integral equation procedure to solve the FGBVP. However, the strong nature of the singularities demanding Cauchy's principal integral values turned out to be a serious obstacle, see Freeden and Gerhards [13]. Later, Freeden and Kersten [14] proposed a new concept of approximations using the generalized Fourier expansions to transfer strongly singular integrals into regular ones. This approach has been further developed in Freeden [12], Bauer [2], Gutting [18], [19], Freeden and Michel [15], Freeden and Gerhards [13]. Recently, Freeden and Nutz [16] published the conceptual setup of the Runge-Walsh theorem for the oblique derivative problem of physical geodesy.

A boom of high-performance computing facilities has brought new opportunities in the field of numerical solutions of various engineering problems. Efficient numerical methods such as the boundary element method (BEM), the finite element method (FEM) or the finite volume method (FVM) can be also applied for gravity field modelling. Main advantages of these approaches are a straightforward refinement of the discretization, opportunity to consider real topography and feasibility for high-resolution modelling.

The BEM applied to gravity field modelling has been widely studied in recent years, see, e.g., Klees [22], Lehmann and Klees [25], Klees et al. [23], Čunderlík et al. [7] or Čunderlík and Mikula [8]. The oblique derivative problem treated by BEM was discussed in Čunderlík et al. [9]. The first application of FVM has been introduced by Fašková [10] and its parallel implementation by Minarechová et al. [35]. However, both papers have studied the geodetic BVP with the Neumann BC. The first insight of FVM applied to the oblique derivative BVP has been discussed in Macák et al. [29]. Later this effort was further developed in Macák et al. [30] and Macák et al. [28], where a treatment of the oblique derivative by the central scheme and the first order upwind scheme, respectively, were introduced for solving FGBVPs on uniform grids. Recently, Medľa et al. [33] presented the FVM for solving the oblique derivative BVP on non-uniform grids. The FEM applied to gravity field modelling has been innovatively studied in Meissl [34], then in Shaofeng and Dingbo [39], Fašková et al. [11], Šprlák at al [40], Mráz et al. [37]. However, none of these approaches has considered the oblique derivative BC in their concepts. On the other hand, the FEM for elliptic partial differential equations with the oblique derivative BC on 2D curved domains has been studied in [1] and recently in [21] and [17].

This paper has two objectives. First, we propose and analyse a finite element approximation of a Laplace equation holding on a domain Ω with an oblique derivative BC given on a part of its boundary $\partial\Omega$. The second objective of the paper is to apply the proposed numerical scheme to local gravity field modelling.

2. Formulation of the oblique derivative BVP

Let us consider the FGBVP, cf. [5, 20, 24]:

$$\Delta T(\mathbf{x}) = 0, \qquad \mathbf{x} \in R^3 - S, \tag{1}$$

$$\nabla T(\mathbf{x}) \cdot \mathbf{s}(\mathbf{x}) = -\delta g(\mathbf{x}), \qquad \mathbf{x} \in \partial S, \tag{2}$$

$$T(\mathbf{x}) \to 0, \quad \text{as} \quad |\mathbf{x}| \to \infty, \tag{3}$$

where S is the Earth or more generally a Lipschitz domain, $T(\mathbf{x})$ is the disturbing potential defined as a difference between the real and normal gravity potential at any point $\mathbf{x} = (x, y, z)$, $\delta g(\mathbf{x})$ is the gravity disturbance that is given and vector $\mathbf{s}(\mathbf{x})$ computed as $\mathbf{s}(\mathbf{x}) = -\nabla U(\mathbf{x})/|\nabla U(\mathbf{x})|$ is the unit vector normal to the equipotential surface of the normal potential $U(\mathbf{x})$ at any point $\mathbf{x}$.

Eqs. (1)–(3) represent an exterior BVP for the Laplace equation, i.e., the computational domain (outside the Earth) is infinite.

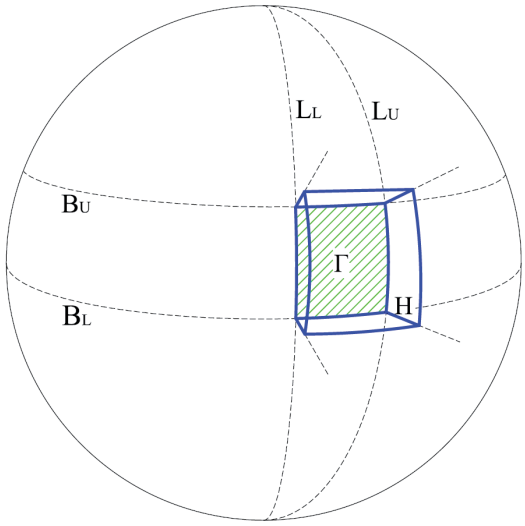

FIGURE 1. The computational domain Ω. The domain Ω is delimited by blue edges; the bottom surface $\Gamma \subset \partial\Omega$ hatched by green colour represents a chosen part of the Earth's surface; B, L, H coordinates denote ellipsoidal latitude, longitude and height, respectively; L, U indexes label lower and upper bounds.

On the other hand, FEM requires a discretization of the whole computational domain into finite elements. To that goal we construct a bounded domain Ω in the external space above the Earth, see [11]. Such a domain Ω (Fig. 1) is bounded by the bottom surface $\Gamma \subset \partial\Omega$ representing a part of the Earth's surface and

an upper surface created at appropriate altitude, e.g., at mean altitude of the GOCE satellite orbits and side boundaries. Then on the top and side boundaries the Dirichlet-type BC for disturbing potential can be generated from any GOCE--based satellite-only geopotential model [32].

In the bounded domain Ω, we consider the following BVP

$$\Delta T(\mathbf{x}) = 0, \qquad \mathbf{x} \in \Omega \subset \mathbb{R}^3, \tag{4}$$

$$\nabla T(\mathbf{x}) \cdot \mathbf{s}(\mathbf{x}) = -\delta g(\mathbf{x}), \qquad \mathbf{x} \in \Gamma \subset \partial\Omega, \tag{5}$$

$$T(\mathbf{x}) = T_{SAT}(\mathbf{x}), \quad \mathbf{x} \in \partial\Omega - \Gamma, \tag{6}$$

where $\Gamma \subset \partial\Omega$ represents the part of the Earth's topography, $\partial\Omega - \Gamma$ represents the top boundary together with side boundaries, and T_{SAT} is the disturbing potential generated from any GOCE-based satellite-only geopotential model.

3. Derivation of the weak formulation of the oblique derivative BVP

To derive the variational formulation of (4)–(6), we define the Sobolev space of test functions V, i.e., the space of functions from $W_2^{(1)}(\Omega)$ which are equal to 0 on $\partial\Omega - \Gamma$ in the sense of traces [6]. We multiply the differential equation (4) by $w \in V$ and using Green's identity (we omit $(\mathbf{x})$ to simplify the notation in the following equations) we get

$$\int_\Omega \nabla T \cdot \nabla w \,\mathrm{d}x\mathrm{d}y\mathrm{d}z = \int_{\partial\Omega} \nabla T \cdot \mathbf{n}\, w \,\mathrm{d}\sigma, \quad w \in V. \tag{7}$$

Now we split the oblique vector $\mathbf{s}$ into one normal and two tangential components

$$\mathbf{s} = c_1\mathbf{n} + c_2\mathbf{t}_1 + c_3\mathbf{t}_2, \tag{8}$$

where $\mathbf{n}$ is the normal vector and $\mathbf{t}_1$, $\mathbf{t}_2$ are tangent vectors to $\Gamma \subset \partial\Omega \subset R^3$. These three vectors together form an orthonormal basis.

Then we put (8) into (5) to obtain

$$\nabla T \cdot \mathbf{s} = c_1 \nabla T \cdot \mathbf{n} + c_2 \nabla T \cdot \mathbf{t}_1 + c_3 \nabla T \cdot \mathbf{t}_2 = -\delta g. \tag{9}$$

From (9) we express the normal derivative

$$\nabla T \cdot \mathbf{n} = \frac{-\delta g}{c_1} - \frac{c_2}{c_1}\frac{\partial T}{\partial \mathbf{t}_1} - \frac{c_3}{c_1}\frac{\partial T}{\partial \mathbf{t}_2} \tag{10}$$

and we insert it to (7) to get

$$\int_\Omega \nabla T \cdot \nabla w \,\mathrm{d}x\mathrm{d}y\mathrm{d}z = \int_\Gamma \left(\frac{-\delta g}{c_1} - \frac{c_2}{c_1}\frac{\partial T}{\partial \mathbf{t}_1} - \frac{c_3}{c_1}\frac{\partial T}{\partial \mathbf{t}_2} \right) w \,\mathrm{d}\sigma. \tag{11}$$

Let the extension of the Dirichlet BC (6) given by T_{SAT} into the domain Ω be in $W_2^{(1)}(\Omega)$ and let $\delta g \in L^2(\Gamma)$. Then we define the weak formulation of BVP as follows: we look for a function T, $T \in W_2^{(1)}(\Omega)$, such that $T - T_{SAT} \in V$ and

$$\int_\Omega \nabla T \cdot \nabla w \,\mathrm{d}x\mathrm{d}y\mathrm{d}z + \frac{c_2}{c_1} \int_\Gamma \frac{\partial T}{\partial \mathbf{t}_1} w \,\mathrm{d}\sigma + \frac{c_3}{c_1} \int_\Gamma \frac{\partial T}{\partial \mathbf{t}_2} w \,\mathrm{d}\sigma = \int_\Gamma \frac{-\delta g}{c_1} w \,\mathrm{d}\sigma, \quad (12)$$

for all $w \in W_2^{(1)}(\Omega)$. The study of weak solution of the oblique derivative BVP is included in the book by Lieberman [27].

4. Solution by the Finite Element Method

The FEM is a numerical method that assumes discretization of the whole computational domain by a union of a collection of elements. For our two-dimensional numerical experiments, we will use three nodes linear triangular and four nodes bilinear quadrilateral elements. For a three-dimensional problem, we use hexahedral elements with eight nodes [6]. A discretization of circular and spherical domains by polygonal elements results in the so-called discretization error that can be partially eliminated using finer discretization. Therefore, repeated refining a mesh will cause the convergence of the finite element domain to the original one.

If we write

$$T^n = \sum_{j=1}^{n} T_j \psi_j, \quad (13)$$

i.e., we take an approximation of T as T^n, a linear combination of basis functions with coefficients T_i, $i = 1, \ldots, n$, then plug it into the weak formulation (12) and consider test function $w = \psi_i$ we get

$$\sum_{j=1}^{n} T_j \left(\int_\Omega \frac{\partial \psi_j}{\partial x}\frac{\partial \psi_i}{\partial x} + \frac{\partial \psi_j}{\partial y}\frac{\partial \psi_i}{\partial y} + \frac{\partial \psi_j}{\partial z}\frac{\partial \psi_i}{\partial z} \,\mathrm{d}x\mathrm{d}y\mathrm{d}z + \right.$$
$$\left. \frac{c_2}{c_1} \int_\Gamma \frac{\partial \psi_j}{\partial \mathbf{t}_1} \psi_i \,\mathrm{d}x\mathrm{d}y + \frac{c_3}{c_1} \int_\Gamma \frac{\partial \psi_j}{\partial \mathbf{t}_2} \psi_i \,\mathrm{d}x\mathrm{d}y \right) = \int_\Gamma \frac{-\delta g}{c_1} \psi_i \,\mathrm{d}x\mathrm{d}y. \quad (14)$$

Properties of ψ_i are as follows. In one-dimensional problem, for each node N_i with coordinate x_i we choose the piecewise linear function ψ_i whose value is

equal to 1 at N_i and 0 at every N_j, $i \neq j$, i.e.,

$$\psi_i = \begin{cases} \frac{x - x_{i-1}}{x_i - x_{i-1}} & \text{if } x \in [x_{i-1}, x_i], \\ \frac{x_{i+1} - x}{x_{i+1} - x_i} & \text{if } x \in [x_i, x_{i+1}], \\ 0, & \text{otherwise,} \end{cases} \qquad \text{for } i = 1, \ldots, n. \tag{15}$$

In two- and three-dimensional problems, we follow the same way, i.e., we choose one basis function ψ_i per vertex N_i. Then the function ψ_i is uniquely determined by choosing value 1 at N_i and 0 at every $N_j, i \neq j$.

Now to calculate the integral over a computational domain Ω in Eq. (14), we use the standard FEM procedure. We choose the type of the element depending on the dimension of the problem and we differentiate the corresponding basis functions with respect to a position of each node in cartesian coordinates.

To calculate two integrals over a boundary Γ in Eq. (14) which include a tangential derivative, we approximate derivatives in tangential direction like in the finite difference method (see Fig. 2 b)), i.e., using values of basis functions at nodes N_i of element e we have

$$\frac{\partial \psi_j^{(e)}}{\partial \mathbf{t}_1} \approx \frac{\psi_j^{(e)}(N_3) - \psi_j^{(e)}(N_1)}{d(N_1, N_3)}, \tag{16}$$

$$\frac{\partial \psi_j^{(e)}}{\partial \mathbf{t}_2} \approx \frac{\psi_j^{(e)}(N_4) - \psi_j^{(e)}(N_2)}{d(N_2, N_4)}, \tag{17}$$

where d denotes the distance between nodes, i.e., length of diagonal of side of the element e that lies on boundary Γ.

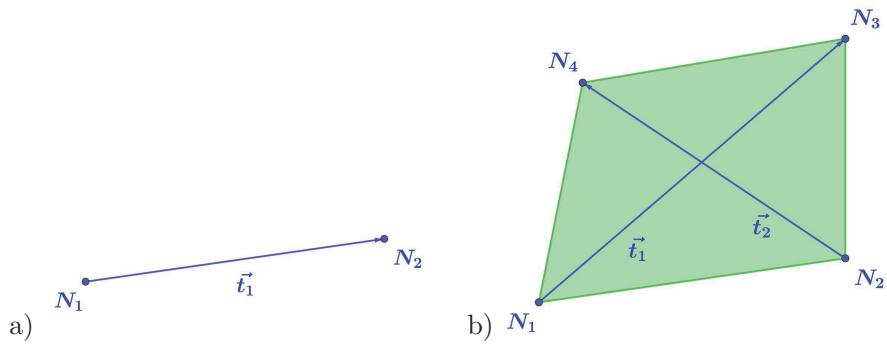

FIGURE 2. Illustration of tangent vectors to botom boundary Γ, when computational domain Ω is a) two-dimensional, b) three-dimensional. By N_i we denote nodes.

Now let $\int_\Gamma \frac{-\delta g}{c_1}\psi_i \,\mathrm{d}x\mathrm{d}y$ be denoted by Q_i, then the column vectors $(T_1,\ldots,T_n)$ and $(Q_1,\ldots,Q_n)$ we denote by $\mathbf{T}$ and $\mathbf{Q}$, respectively, where derivatives in tangential direction are approximated using (16) and (17). Let $\mathbf{K}=[K_{ij}]$ be matrix whose entries are

$$K_{ij}=\int\limits_\Omega \nabla\psi_j\cdot\nabla\psi_i \,\mathrm{d}x\mathrm{d}y\mathrm{d}z+\frac{c_2}{c_1}\int\limits_\Gamma \frac{\partial\psi_j}{\partial\mathbf{t}_1}\psi_i \,\mathrm{d}x\mathrm{d}y+\frac{c_3}{c_1}\int\limits_\Gamma \frac{\partial\psi_j}{\partial\mathbf{t}_2}\psi_i \,\mathrm{d}x\mathrm{d}y, \tag{18}$$

then we may rephrase (14) as

$$\mathbf{KT}=\mathbf{Q}. \tag{19}$$

It represents the linear system of equations for unknown nodal solution values T. The matrix $\mathbf{K}$ is usually referred to as the stiffness matrix which is sparse since most of its entries are zero and, in addition, the matrix is positive definite.

5. Numerical experiments

To illustrate the numerical method to cope with an oblique derivative condition we present various experiments implemented in MATLAB software [31]. In them, results of FEM solutions will be compared to either exact (testing experiments) or EGM 2008 (experiments with gravity data) solutions. Then the standard deviations of differences between numerical solutions denoted by T_{FEM} and the exact solution or EGM 2008 value denoted by T_{exact} will be defined as

$$\sigma_{\mathrm{num}}=\sqrt{\frac{1}{n}\sum_{i=1}^{n}(T_{\mathrm{FEM}_i}-T_{\mathrm{exact}_i})^2}, \tag{20}$$

where n is the number of nodes.

Afterwards the numerical scheme will be qualified according to the value of the so-called experimental order of convergence (EOC). In general, EOC can be computed as follows. Let us have the grid size h. In FEM approach the grid size will be the size of elements, so in 1D — the length of element, in 2D — the area of the element and in 3D — the volume of element. If we assume that the error of the scheme in some norm is proportional to some power of the grid size, i.e., $\mathrm{Error}(h)=ch^\varepsilon$, with a constant c, then having two grids with sizes h_1 and h_2, where $h_1>h_2$, yields two errors $\mathrm{Error}(h_1)=c(h_1)^\varepsilon$ and $\mathrm{Error}(h_2)=c(h_2)^\varepsilon$ from where we can simply extract

$$\varepsilon=\log_{\frac{h_1}{h_2}}\left(\frac{\mathrm{Error}(h_1)}{\mathrm{Error}(h_2)}\right). \tag{21}$$

If $h_2 = \frac{h_1}{2}$ we can simplify

$$\varepsilon = \log_2 \left(\frac{\text{Error}(h_1)}{\text{Error}(h_2)} \right). \tag{22}$$

Then the value ε is EOC and it can be determined by comparing numerical solutions and exact solutions on subsequently refined grids.

5.1. Testing numerical experiments

In the following numerical experiments, we have simulated the oblique vector in the oblique derivative BC by rotating this vector or/and by shifting the center of gravity of the computational domain which will be denoted by C (see Fig. 3).

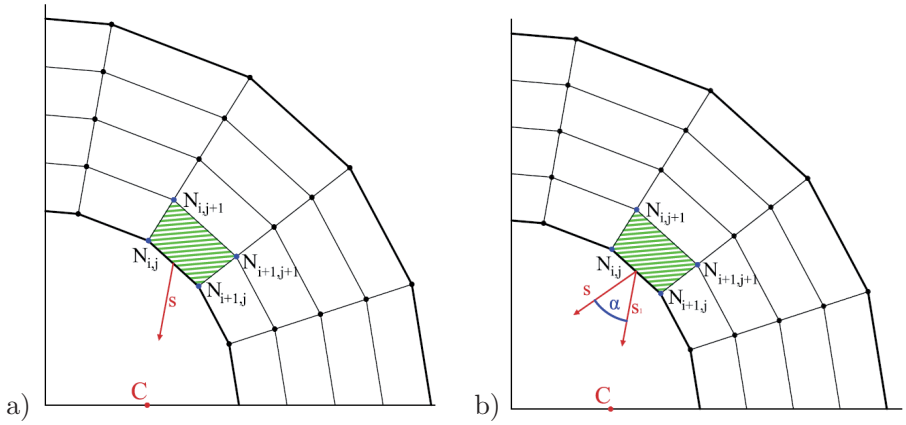

FIGURE 3. Illustration of the 2D FEM grid on a sector of a circle. The oblique vector $\vec{s}$ depicted by red arises from a) a shift of the center C of the computational domain, b) a shift of the center C of the computational domain and a rotation by an angle $\pm\alpha$. The $\pm\alpha$ means that on one element we modify the vector $\vec{s}$ by a value $+\alpha$ and on its adjacent elements by $-\alpha$.

5.1.1. Experiment 1: 2D computational domain - a square

The computational domain has been the rectangular region — a square bounded by cartesian coordinates

$$x_1 = -1.0\,[m], \quad x_2 = 1.0\,[m], \quad y_1 = 1.0\,[m] \quad \text{and} \quad y_2 = 3.0\,[m].$$

The center C for calculating BC has been shifted to $C = [0.2, 0]$. For these numerical experiments, we used three nodes linear triangular as well as four nodes bilinear quadrilateral elements. As the Dirichlet BC (6) on the upper and side boundaries, the chosen exact solution of (4) in the form $T_{\text{exact}} = -\log r$, where r is the distance from the C, has been applied. Then we have tested two cases:

a) *oblique vector caused by a shift of the center C*

As the oblique derivative BC on the bottom boundary, derivative of this exact solution in direction of its gradient, which is equal to $-1/r$, has been considered. The σ_{num} and EOC for subsequently refined grids can be found in Table 1. One can observe that the numerical method is approximately of the second order for both types of elements.

TABLE 1. σ_{num} and EOC for *Experiment 1 a)*. Domain bounded by: $x_1 = -1.0\,[m]$, $x_2 = 1.0\,[m]$, $y_1 = 1.0\,[m]$ and $y_2 = 3.0\,[m]$; center C shifted to $C = [0.2, 0]$; angle $\alpha = 0\,[\text{deg}]$.

No. of nodes	Triangular el.		Quadrilateral el.	
$n_1 \times n_2$	σ_{num}	EOC	σ_{num}	EOC
4×4	0.062932	—	0.012371	—
8×8	0.012204	2.366397	0.001784	2.793944
16×16	0.002687	2.183517	0.000343	2.379069
32×32	0.000631	2.091020	0.000075	2.183775
64×64	0.000153	2.045292	0.000018	2.090428
128×128	0.000038	2.022590	0.000004	2.044818

b) *oblique vector obtained by adding an angle* $\pm\alpha$

We had the same computational domain and BC on the upper and side boundaries, but the direction of the original vector $\mathbf{s}_1$ has been modified by an angle α to create a new unit vector $\mathbf{s}$, see Fig. 3 b). For this experiment we have chosen $\alpha = 5\,[\text{deg}]$ (Table 2) and $\alpha = 60\,[\text{deg}]$ (Table 3). Then the oblique derivative BC was given by the projection $\nabla T \cdot \mathbf{s} = -(1/r)\cos(\alpha)$. As we can see in Table 2 and Table 3, the EOC of the scheme for small values of an angle α is approximately two, however for larger values of α significantly varies in values.

5.1.2. Experiment 2: 2D computational domain - sector of an annulus

Now the computational domain has been the circular region - a sector of an annulus bounded by polar coordinates $r_1 = 1.0\,[m]$, $r_2 = 2.0\,[m]$, $\phi_1 = 0\,[\text{deg}]$ and $\phi_2 = 90\,[\text{deg}]$. The center C for simulating the oblique vector in BC has been shifted to $C = [0.5, 0.35]$. We used four nodes bilinear quadrilateral elements. As the Dirichlet BC (6) on the upper and side boundaries the exact solution of (4) in the form $T_{\text{exact}} = -\log r$, where r is the distance from the C, has been applied. Then we had two cases:

TABLE 2. σ_{num} and EOC for *Experiment 1 b)*. Domain bounded by: $x_1 = -1.0\,[m]$, $x_2 = 1.0\,[m]$, $y_1 = 1.0\,[m]$ and $y_2 = 3.0\,[m]$; center $C = [0, 0]$; angle $\alpha = 5\,[\text{deg}]$.

No. of nodes	Triangular el.		Quadrilateral el.	
$n_1 \times n_2$	σ_{num}	EOC	σ_{num}	EOC
4×4	0.062945	—	0.014058	—
8×8	0.011988	2.392471	0.002105	2.739195
16×16	0.002661	2.171835	0.000446	2.239504
32×32	0.000637	2.062288	0.000118	1.914739
64×64	0.000162	1.974415	0.000038	1.650359
128×128	0.000045	1.845852	0.000012	1.624698

TABLE 3. σ_{num} and EOC for *Experiment 1 b)*. Domain bounded by: $x_1 = -1.0\,[m]$, $x_2 = 1.0\,[m]$, $y_1 = 1.0\,[m]$ and $y_2 = 3.0\,[m]$; center $C = [0, 0]$; angle $\alpha = 60\,[\text{deg}]$.

No. of nodes	Triangular el.		Quadrilateral el.	
$n_1 \times n_2$	σ_{num}	EOC	σ_{num}	EOC
4×4	0.661526	—	0.151381	—
8×8	0.301333	1.134438	8.477170	-5.807325
16×16	0.095939	1.651172	0.102618	6.368233
32×32	0.050959	0.912768	0.054637	0.909319
64×64	0.035304	0.529502	0.009881	2.467113
128×128	0.011227	1.652923	0.005974	0.725969

a) *oblique vector forced by a shift of the center C*

As the oblique derivative BC on the bottom boundary, derivative of the exact solution in direction of its gradient, which is equal to $1/r$, has been considered. The σ_{num} and EOC for subsequently refined grids can be found in Table 4. One can observe that the numerical method is approximately of the second order.

b) *oblique vector forced by a shift of the center C and a rotation by an angle* $\pm\alpha$

Now the direction of the original vector $\mathbf{s}_1$ has been modified by an angle $\alpha = 5\,[\text{deg}]$ and $\alpha = 60\,[\text{deg}]$.

As we can see in Table 5, again for small values of α the proposed method is second order accurate, while for large values of α, the EOC varies.

TABLE 4. σ_{num} and EOC for *Experiment 2 a)*. Domain bounded by: $r_1 = 1.0\,[m]$, $r_2 = 2.0\,[m]$, $\phi_1 = 0\,[\text{deg}]$ and $\phi_2 = 90\,[\text{deg}]$; center C shifted to $C = [0.5, 0.35]$.

$n_1 \times n_2$	σ_{num}	EOC
4×4	0.013438	—
8×8	0.001811	2.891751
16×16	0.000372	2.281669
32×32	0.000086	2.120233
64×64	0.000021	2.056062
128×128	0.000005	2.027059

TABLE 5. σ_{num} and EOC for *Experiment 2 b)*. Domain bounded by: $r_1 = 1.0\,[m]$, $r_2 = 2.0\,[m]$, $\phi_1 = 0\,[\text{deg}]$ and $\phi_2 = 90\,[\text{deg}]$; center C shifted to $C = [0.5, 0.35]$; angle $\alpha = 5\,[\text{deg}]$, $\alpha = 60\,[\text{deg}]$.

No. of nodes	$\alpha = 5\,[\text{deg}]$		$\alpha = 60\,[\text{deg}]$	
$n_1 \times n_2$	σ_{num}	EOC	σ_{num}	EOC
4×4	0.015301	—	0.037844	—
8×8	0.001843	3.053115	0.005124	2.884784
16×16	0.000375	2.297875	0.002349	1.125313
32×32	0.000086	2.120392	0.001176	0.998145
64×64	0.000021	2.056354	0.000391	1.590127
128×128	0.000005	2.027237	0.000119	1.716936

5.1.3. Experiment 3: 3D computational domain - a cube

The computational domain has been the rectangular region - a cube bounded by artesian coordinates $x_1 = -2.0\,[m]$, $x_2 = 2.0\,[m]$, $y_1 = -2.0\,[m]$, $y_2 = 2.0\,[m]$ and $z_1 = 1.0\,[m]$, $z_2 = 5.0\,[m]$. The center C has been shifted to $C = [-3, -5, 0]$. To mesh the computational domain Ω, we used hexahedral elements with eight nodes. As the Dirichlet BC (6) we have considered the exact solution of (4) in the form $T_{\text{exact}} = 1/r$, where r is the distance from the center point C. So the oblique vector in oblique derivative BC was a result of:

a) *a shift of the center C*

As the oblique BC on the bottom boundary, we have supposed the derivative of this exact solution that is equal to $-1/r^2$. The results can be seen in Table 6. One can see that the proposed approach is second order accurate.

TABLE 6. σ_{num} and EOC for *Experiment 3 a)*. Domain bounded by cartesian coordinates $x_1 = -2.0\,[m]$, $x_2 = 2.0\,[m]$, $y_1 = -2.0\,[m]$, $y_2 = 2.0\,[m]$, $z_1 = 1.0\,[m]$ and $z_2 = 5.0\,[m]$; the center C shifted to $C = [-3, -5, 0]$.

$n_1 \times n_2 \times n_3$	σ_{num}	EOC
$4 \times 4 \times 4$	0.000356	—
$8 \times 8 \times 8$	0.000051	2.793095
$16 \times 16 \times 16$	0.000009	2.531285
$32 \times 32 \times 32$	0.000002	2.274487
$64 \times 64 \times 64$	0.000000	2.121095

b) *a shift of the center C and rotation by an angle $\pm\alpha$*

For the second testing experiment on cube we had the same computational domain and the same BCs as in the previous one, but the oblique vector $\mathbf{s}$ has been rotated by 5 [deg] and 60 [deg]. The standard deviations of differences between numerical solutions and the exact solution as well as the EOC of the method are shown in Table 7. One can see that also in this case with the rotated oblique vector, the method for small values of α works.

TABLE 7. σ_{num} and EOC for *Experiment 3 b)*. Domain bounded by cartesian coordinates $x_1 = -1.0\,[m]$, $x_2 = 1.0\,[m]$, $y_1 = -1.0\,[m]$, $y_2 = 1.0\,[m]$, $z_1 = 1.0\,[m]$ and $z_2 = 3.0\,[m]$; $C = [-3, -5, 0]$; angle $\alpha = 5$ [deg], 60 [deg].

No. of nodes	$\alpha = 5$ [deg]		$\alpha = 60$ [deg]	
$n_1 \times n_2 \times n_3$	σ_{num}	EOC	σ_{num}	EOC
$4 \times 4 \times 4$	0.000357	—	0.005943	—
$8 \times 8 \times 8$	4.981552e-05	2.841373	0.000049	6.916226
$16 \times 16 \times 16$	8.405654e-06	2.567163	0.000160	-1.697974
$32 \times 32 \times 32$	1.702424e-06	2.303770	0.044522	-8.123485
$64 \times 64 \times 64$	3.864044e-07	2.139407	382.506193	-13.068668

5.1.4. Experiment 4: 3D computational domain - tesseroid

Now the computational domain has been a tesseroid bounded by two concentric spheres with radii $r_1 = 1$ and $r_2 = 2$, and a coaxial cone with dimension $(0, \pi/4) \times (0, \pi/4)$. As the Dirichlet BC (6) on the upper and side boundaries, we have considered the exact solution of (4) in the form $T_{\text{exact}} = 1/r$, where r is the distance from the center point C.

a) *shift of the center C*

The center point has been shifted to $C = [0.1, -0.1, 0.1]$. As the oblique derivative BC on the bottom boundary, we have supposed the derivative of this exact solution, i.e., $-1/r^2$. The results can be seen in Table 8. One can see that the proposed approach is second order accurate.

TABLE 8. σ_{num} and EOC for *Experiment 4 a)*. Domain bounded by: $r_1 = 1$ and $r_2 = 2$, and a coaxial cone with dimension $(-\pi/4, \pi/4) \times (-\pi/4, \pi/4)$; the center C shifted to $C = [0.1, -0.1, 0.1]$.

$n_1 \times n_2 \times n_3$	σ_{num}	EOC
$4 \times 4 \times 4$	0.001652918715	—
$8 \times 8 \times 8$	0.000295750289	2.482564
$16 \times 16 \times 16$	0.000058914678	2.327681
$32 \times 32 \times 32$	0.000013188810	2.159313
$64 \times 64 \times 64$	0.000003011359	2.130838

b) *shift of the center C and a rotation by an angle* $\pm\alpha$

The center C has been shifted to $C = [0.2, -0.3, -0.2]$ and the oblique vector $\mathbf{s}$ has been modified by an angle $\alpha = \pm 5\,[\text{deg}]$ and then by $\alpha = \pm 60\,[\text{deg}]$. The standard deviations of differences between numerical solutions and the exact solution as well as the EOC of the method are shown in Table 9. The method performed as we have expected.

TABLE 9. σ_{num} and EOC for *Experiment 4 b)*. Domain bounded by: $r_1 = 1$ and $r_2 = 2$, and a coaxial cone with dimension $(-\pi/4, \pi/4) \times (-\pi/4, \pi/4)$; the center C shifted to $C = [0.2, -0.3, -0.2]$; angle $\alpha = \pm 5\,[\text{deg}]$, $\alpha = \pm 60\,[\text{deg}]$.

No. of nodes	$\alpha = 5\,[\text{deg}]$		$\alpha = 60\,[\text{deg}]$	
$n_1 \times n_2 \times n_3$	σ_{num}	EOC	σ_{num}	EOC
$4 \times 4 \times 4$	0.001664616019	—	0.001354338745	—
$8 \times 8 \times 8$	0.000297491470	2.484269	0.000171918671	2.977790
$16 \times 16 \times 16$	0.000059232690	2.328383	0.000029014762	2.566867
$32 \times 32 \times 32$	0.000013232627	2.162294	0.000023208962	0.322105
$64 \times 64 \times 64$	0.000003260503	2.020933	0.000024858690	-0.099068

c) *Oblique vector has a constant direction on every element.*

Now the we had the constant oblique vector $\mathbf{s} = [-0.5\,{-1}\,{-0.5}]$. The results can be seen in Table 10. One can see that the proposed approach for a constant oblique vector $\mathbf{s}$ is second order accurate.

TABLE 10. σ_{num} and EOC for *Experiment 4 c)*. Domain bounded by: $r_1 = 1$ and $r_2 = 2$, and a coaxial cone with dimension $(-\pi/4, \pi/4) \times (-\pi/4, \pi/4)$; Oblique vector $\mathbf{s} = [-0.5, -1, -0.5]$.

$n_1 \times n_2 \times n_3$	σ_{num}	EOC
$4 \times 4 \times 4$	0.002545212860	—
$8 \times 8 \times 8$	0.000435216353	2.547982
$16 \times 16 \times 16$	0.000083234911	2.386472
$32 \times 32 \times 32$	0.000018016813	2.207845
$64 \times 64 \times 64$	0.000004189318	2.104557

5.2. Numerical experiments with gravity data

Numerical experiments with gravity data were performed in the domain above the Himalayas bounded by $\langle 60, 110\rangle$ meridians and $\langle 20, 50\rangle$ parallels, i.e., in the computational grid above the extremely complicated Earth's topography. The bottom boundary was given by grid points that were located on the Earth's surface and their spacing in horizontal directions was uniform. Their heights were interpolated from the SRTM 30 PLUS topography model [3]. An upper boundary was chosen in the height of 240 km above a reference ellipsoid WGS84 corresponding to an average altitude of the GOCE satellite orbits. The EGM 2008 based on spherical harmonic up to degree 2160 [38] was used to generate all BCs. On the bottom boundary, the first derivatives in the radial direction were prescribed. They represented the oblique derivative BC. On the rest of the boundary, the Dirichlet BC in form of the disturbing potential was prescribed. Then three experiments with different grid densities were performed, namely the grids with the densities $76 \times 126 \times 5$, $151 \times 251 \times 9$ and $301 \times 501 \times 17$. These grids approximately correspond to spacing 0.4 [deg] $\times\, 0.4$ [deg] $\times\, 60$ [km], 0.2 [deg] $\times\, 0.2$ [deg] $\times\, 30$ [km] and 0.1 [deg] $\times\, 0.1$ [deg] $\times\, 15$ [km], respectively.

The statistical characteristics of the corresponding residuals are summarized in Table 11 and Fig 4. It is evident that refinements of the grid lead to higher accuracy of the FEM solution giving a better agreement with EGM 2008.

TABLE 11. *Numerical experiments with gravity data* — The statistical characteristics of residuals computed as $res_i = T_{FEM_i} - T_{\text{exact}_i}$ $[m^2 s^{-2}]$, $i = 1, \ldots n$, where n is the number of nodes.

Grid density:	$76 \times 126 \times 5$	$151 \times 251 \times 9$	$301 \times 501 \times 17$
Min. res.	-51.609	-25.090	-8.200
Max. res.	42.950	12.060	3.130
Mean res.	-0.864	-0.960	-0.231
σ_{num}	6.193	2.469	0.694

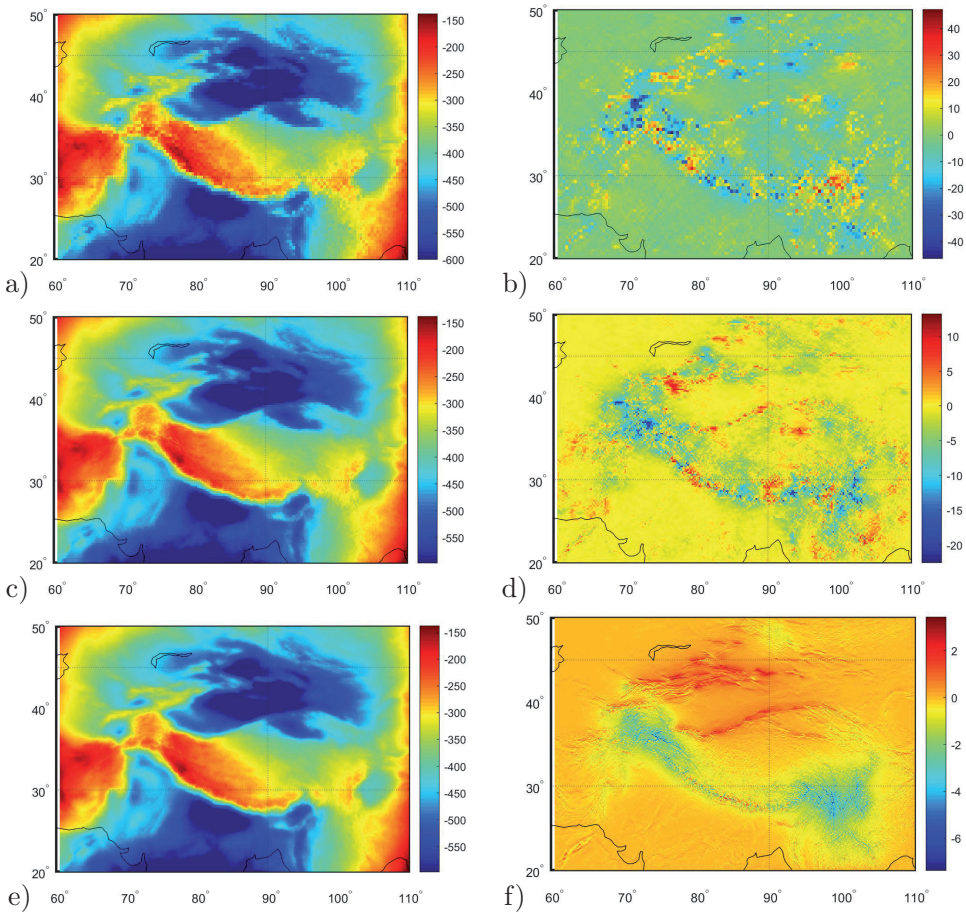

FIGURE 4. a), c), e) The disturbing potential from our FEM solution; b),d),f) residuals between the EGM2008 and FEM solution, where grid density is a),b) $76 \times 126 \times 5$, c),d) $151 \times 251 \times 9$, e),f) $301 \times 501 \times 17$ points $[m^2 s^{-2}]$.

6. Concluding remarks

In this paper, we have derived an original numerical scheme to approximate the solution of the Laplace equation with an oblique derivative boundary condition by the finite element method. We have tested this approach in various two- and three-dimensional testing numerical experiments. They have showed that for small rotations of oblique vector, the proposed scheme is second order accurate. Then we have applied it to gravity field modelling in Himalayas. The numerical experiments have demonstrated that the proposed approach is able to reconstruct a harmonic function.

REFERENCES

[1] BARRETT, J. W.—ELLIOTT, CH. M.: *Fixed mesh finite element approximations to a free boundary problem for an elliptic equation with an oblique derivative boundary condition*, Compt. Math. Appl. **11** (1985), no. 4, 335–345.

[2] BAUER, F.: *An Alternative Approach to the Oblique Derivative Problem in Potential Theory*. In: PhD Thesis, Geomathematics Group, Department of Mathematics, University of Kaiserslautern, Shaker Verlag, Aachen, Germany, 2004.

[3] BECKER, J. J.—SANDWELL, D. T.—SMITH, W. H. F.—BRAUD, J.—BINDER, B.—DEPNER, J.—FABRE, D.—FACTOR, J.—INGALLS, S.—KIM S. H.—LADNER, R.—MARKS, K.—NELSON, S.—PHARAOH, A.—TRIMMER, R.—ROSENBERG, J. VON, WALLACE, G.—WEATHERALL, P.: *Global bathymetry and elevation data at 30 arc seconds resolution: SRTM30 PLUS*, Marine Geodesy **32** (2009), no. 4, 355–371.

[4] BITZADSE, A. V.: *Boundary-Value Problems for Second-Order Elliptic Equations*. North-Holland, Amsterdam, 1968.

[5] BJERHAMMAR, A.—SVENSSON, L.: *On the geodetic boundary value problem for a fixed boundary surface, A satellite approach*, Bull Geod. **57** (1983), no. 1–4, 382–393.

[6] BRENNER, S. C.—SCOTT, L. R.: *The Mathematical Theory of Finite Element Methods*. Springer-Verlag, New York, 2002.

[7] ČUNDERLÍ K, R.—MIKULA, K.—MOJZEŠ, M.: *Numerical solution of the linearized fixed gravimetric boundary-value problem*, J. Geod. **82** (2008), 15–29.

[8] ČUNDERLÍ K, R.—MIKULA, K.: *Direct BEM for high-resolution gravity field modelling*, Stud. Geophys. Geod. **54** (2010), no. 2, 219–238

[9] ČUNDERLÍK, R.—MIKULA, K.—ŠPIR R.: *An oblique derivative in the direct BEM formulation of the fixed gravimetric BVP*, IAG Symp. **137** (2012), 227–231.

[10] FAŠKOVÁ, Z.: *Numerical Methods for Solving Geodetic Boundary Value Problems*. PhD Thesis, SvF STU, Bratislava, Slovakia, 2008.

[11] FAŠKOVÁ, Z.—ČUNDERLÍK, R.—MIKULA, K.: *Finite element method for solving geodetic boundary value problems*, J. Geod. **84** (2010), no. 2, 135–144

[12] FREEDEN, W.: *Harmonic splines for solving boundary value problems of potential theory*. In: J. C. Mason, M. G. Cox, eds.) *Algorithms for Approximation, (Shrivenham, 1985)*, Inst. Math. Appl. Conf. Ser. New Ser. Vol. 10, Oxford Univ. Press, New York, pp. 507–529.

[13] FREEDEN, W.—GERHARDS, C.: *Geomathematically Oriented Potential Theory*, CRC Press (2013)

[14] FREEDEN, W.—KERSTEN, H.: *A constructive approximation theorem for the oblique derivative problem in potential theory*, Mathematical Methods in Appl. Sci. **3** (1981), 104–114.

[15] FREEDEN, W.—MICHEL, V.: *Multiscale Potential Theory. With Applications to Geoscience*. In: *Applied and Numerical Harmonic Analysis*. Birkhäuser Boston, Inc., Boston, MA, 2004.

[16] FREEDEN W.—NUTZ H.: *On the Solution of the Oblique Derivative Problem by Constructive Runge-Walsh Concepts*, In: *Recent Applications of Harmonic Analysis to Function Spaces, Differential Equations, and Data Science*. (I. Pesenson, Q. Le Gia, A. Mayeli, H. Mhaskar, Dx. Zhou, eds.) Applied and Numerical Harmonic Analysis. Birkhäuser, Cham. 2017.

[17] GALLISTL, D.: *Numerical approximation of planar oblique derivative problems in nondivergence form*, Math. Comp. **88** (2019), 1091–1119

[18] GUTTING, M.: *Fast Multipole Methods for Oblique Derivative Problems*. In: PhD Thesis, Geomathematics Group, Department of Mathematics, University of Kaiserslautern. Shaker Verlag, Aachen, Germany 2007.

[19] GUTTING, M.: *Fast multipole accelerated solution of the oblique derivative boundary value problem*, International Journal on Geomathematics **3** (2012), 223–252.

[20] HOLOTA, P.: *Coerciveness of the linear gravimetric boundary-value problem and a geometrical interpretation*, J. Geod. **71** (1997), 640–651.

[21] KAWECKI, E.: *A Discontinuous Galerkin Finite Element Method for Uniformly Elliptic Two Dimensional Oblique Boundary-Value Problems*, SIAM J. Numer. Anal. **57** (2019), no. 2, 751–778.

[22] KLEES, R.: *Boundary value problems and approximation of integral equations by finite elements*, Manuscripta Geodaetica **20** (1995), 345–361.

[23] KLEES, R.—VAN GELDEREN, M.—LAGE, C.—SCHWAB, C.: *Fast numerical solution of the linearized Molodensky problem*, J. Geod. **75** (2001), 349–362.

[24] KOCH, K. R.—POPE, A. J.: *Uniqueness and existence for the geodetic boundary value problem using the known surface of the earth*, Bull. Geod. **46** (1972), 467–476.

[25] LEHMANN, R.—KLEES, R.: *Numerical solution of geodetic boundary value problems using a global reference field*, J. Geod. **73**, (1999), 543–554.

[26] LEVEQUE, R. J.: *Finite Volume Methods for Hyperbolic Problems*. Cambridge Texts in Applied Mathematics, Cambridge University Press, Cambridge, 2002.

[27] LIEBERMAN, G. M.: *Oblique Derivative Problems for Elliptic Equations*. World Scientific Publishing Co. Pte. Ltd., Hackensack, NJ, 2003.

[28] MACÁK, M.—ČUNDERLÍK, R.—MIKULA, K.—MINARECHOVÁ, Z.: *An upwind-based scheme for solving the oblique derivative boundary-value problem related to the physical geodesy*, J. Geod. Sci. **5**, (2015) no. 1, 180–188.

[29] MACÁK, M.—MIKULA, K.—MINARECHOVÁ, Z.: *Solving the oblique derivative boundary-value problem by the finite volume method*. In: 19th Conference on Scientific Computing, Podbanske, Slovakia, September 9-14, 2012, *ALGORITMY 2012* (Proceedings of contributed papers and posters), Publishing House of STU, 2012, pp. 75–84.

[30] MACÁK, M.—MINARECHOVÁ, Z.—MIKULA, K.: *A novel scheme for solving the oblique derivative boundary-value problem*, Stud. Geophy. Geo. **58** (2014), no. 4, 556–570.

[31] *MATLAB version 2018 b*. The MathWorks Inc., Natick, Massachusetts: 2018.

[32] MAYER-GURR, T., ET AL,: *The new combined satellite only model GOCO03s*. In: Presented at the GGHS-2012 in Venice, Italy 2012.

[33] MEDĽA, M.—MIKULA, K.—ČUNDERLÍK, R.—MACÁK, M.: *Numerical solution to the oblique derivative boundary value problem on non-uniform grids above the Earth topography*, J. Geod. DOI 10.1007/s00190-017-1040-z(2017).

[34] MEISSL, P.: *The use of finite elements in physical geodesy*. Report 313. In: *Geodetic Science and Surveying*, The Ohio State University 1981. https://apps.dtic.mil/dtic/tr/fulltext/u2/a104164.pdf

[35] MINARECHOVÁ, Z.—MACÁK, M.—ČUNDERLÍK, R.—MIKULA, K.: *High-resolution global gravity field modelling by the finite volume method*, Stud. Geophys Geo. **59** (2015), 1–20.

[36] MIRANDA, C.: *Partial Differential Equations of Elliptic Type*. Springer-Verlag, Berlin, 1970.

[37] MRÁZ, D.—BOŘÍK, M.—NOVOTNÝ, J.: *On the convergence of the h-p finite element method for solving boundary value problems in physical geodesy*. In: International Symposium on Earth and Environmental Sciences for Future Generations (J. T. Freymueller, L. Sánchez, eds.), *International Association of Geodesy Symposia Vol. 147*, Springer, Cham, Switzerland. 2016, pp. 39–45.

[38] PAVLIS, N.K.—HOLMES, S.A.—KENYON, S.C.—FACTOR, J.K.: *The development and evaluation of the Earth Gravitational Model 2008 (EGM2008)*, Journal of Geophysical Research **117** (2012), B04406. DOI:10.1029/2011JB008916

[39] SHAOFENG, B.—DINGBO, C.: *The finite element method for the geodetic boundary value problem*, Manuscr. Geod. **16** (1991), 353–359.

[40] ŠPRLÁK, M.—FAŠKOVÁ, Z.—MIKULA, K.: *On the application of the coupled finite-infinite element method to the geodetic boundary value problem*, Stud. Geophys. Geo. **55** (2011), 479–487.

Received April 30, 2019

Department of Mathematics and Descriptive Geometry
Faculty of Civil Engineering
Slovak University of Technology in Bratislava
Radlinského 11
SK–810-05 Bratislava
SLOVAKIA

E-mail: marek.macak@stuba.sk
zuzana.minarechova@stuba.sk
cunderli@svf.stuba.sk
karol.mikula@stuba.sk